Experimental Characterization of a new Benchmark Structure for Prediction of Damping Nonlinearity

Aabhas Singh
University of Wisconsin – Madison
singh36@wisc.edu

Matteo Scapolan
Politecnico di Torino
matteo.scapolan@polito.it

Yuta Saito
University of Illinois at Urbana–Champaign
ysaito2@illinois.edu

Matthew S. Allen
University of Wisconsin – Madison
msallen@engr.wisc.edu

Daniel Roettgen
Sandia National Laboratories
drroett@sandia.gov

Ben Pacini
Sandia National Laboratories
brpacin@sandia.gov

Robert Kuether
Sandia National Laboratories
rjkueth@sandia.gov

ABSTRACT

Spacecraft, airplanes, automobiles, machines and civil structures are all constructed from multiple parts joined by bolts, rivets or other fasteners and these joints lead to large uncertainties in the structural stiffness, damping and can even introduce nonlinearity. Even with the best available simulation tools, it is still difficult to predict the effective stiffness and damping of bolted interfaces, and so these parameters are often assumed and updated after tests have been performed. Damping estimates are critical to limit the resonant vibration response of a structure and thus prevent failure. Even so, it remains poorly understood and available methods for modeling damping are inaccurate and computationally expensive. A new benchmark structure has been created that is designed so as to be predictable with current simulation tools. This paper presents a thorough experimental characterization of this new benchmark structure using the Hilbert transform method applied to modally filtered time data. The nonlinear frequency and damping of each mode is characterized for various levels of bolt preload and excitation amplitude. The interfaces of the bolted structure are also characterized in detail by measuring the contact pressure distribution using pressure sensitive film. The resulting data presents a set of well characterized tests that can be used to validate numerical methods that seek to predict the nonlinear behavior of bolted interfaces.

Keywords: Modal testing, modal analysis, Hilbert transform, mechanical interfaces, contact pressure characterization

1. Introduction

The finite element method has developed to the point that one can now create remarkably accurate and predictive models of parts even with complicated and intricate geometry. However, this is only true so long as they are constructed of a single piece of metal. Interfaces between parts of different materials or the same material lead to large uncertainties. Airplanes, automobiles, machines and civil structures are all constructed from multiple parts joined by bolts, rivets or other fasteners and these joints introduce large uncertainties in the structural stiffness, damping and nonlinearity. Even with the best available simulation tools, it is still difficult to predict the effective stiffness and damping of bolted interfaces, and so often these parameters are assumed and updated after tests have been performed. Damping is critical to limit the resonant response of a structure and thus prevent failure, and yet it remains poorly understood and available methods for modeling damping are inaccurate and computationally expensive.

In recent years, test methods have been developed that can accurately describe the nonlinear stiffness and damping of structures with joints, and these have been used to tune models to measurements up to moderately large amplitudes. Recent experimental works by Roettgen et al. [1], and Deaner et al. [2] show that the modes of a structure with joints can remain uncoupled. This characteristic has been used to test several structures to update the corresponding finite element models to describe the nonlinear effects of the joints. Free response time histories have been used for this purpose to allow quick comparisons between these experimental data and simulations from models using some recently developed signal processing and analysis techniques. The amplitude dependent natural frequencies and damping ratios estimated with the Hilbert transform from experimental data, allowing the models to be calibrated using the analysis proposed by Allen et al., [3] and Festjens et al. [4]. The thesis by Lacayo [5] has successfully demonstrated this workflow using the Brake-Reuss (BRB) beam.

Previous work towards understanding the characteristics of the joint nonlinearity in the structural dynamic response has proved successful in correlating Iwan models to the nonlinear characteristics of the Brake – Reuss Beam. This benchmark structure has a square cross-section with a three-bolt lap joint at the center [5]. The work in this paper aims to characterize a beam with a simpler two – bolt joint assembly in an effort to create simpler interfaces to investigate the joints influence on the nonlinear stiffness and damping. This new benchmark structure, termed the “S4 Beam”, features two bolted interfaces at the ends of two c - shaped beams, designed to model the nonlinear effects of joint bending and shearing in bolted structures. The beam structure is depicted below in **Figure 1.1:** The unbolted S4 BeamFigure 1.1.

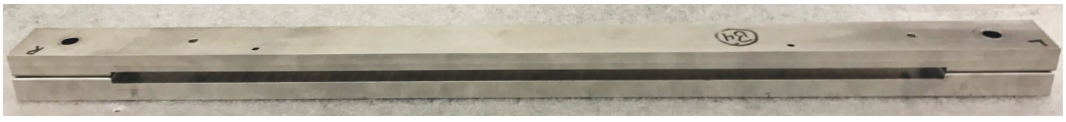

Figure 1.1: *The unbolted S4 Beam*

Prior to the characterization the joint, a comprehensive test sequence is developed to understand the effects of bolt torque level, excitation level, and joint interface curvature on the nonlinear dynamics of the structure. Similarly to the BRB, the Hilbert Transform is used on the free response data to detect the degree of nonlinearity [6]. In addition to the nonlinearity, the joint is characterized by measuring the pressure distribution along the surface of the interface through pressure film measurements taken at various torque levels.

2. Theoretical Background

Experimental modal analysis of a structure is used to identify the linear modal parameters (i.e. shapes, frequencies and damping) of a linear, time invariant system. However, if the system is nonlinear, then nonlinear techniques are needed to characterize the degree of nonlinearity for each mode of the system. In this research, the nonlinearity is characterized numerically using the Hilbert transform. Below is a summary of the Hilbert transform as described by Allen and Roettgen [1].

The Hilbert transform has been widely used for nonlinearity detection for single degree of freedom (SDOF) systems. However, given that the physical measurements ($\ddot{x}(t)$) from accelerometers commonly used in modal testing incorporate coupling when multiple modes are excited for a given input, the measurements are transformed into the modal domain ($\ddot{q}(t)$) using a modal filter to result in modal SDOF systems as described in Kerschen et al. [7]. and as shown in Equation 1.

$$\ddot{x}(t) = \Phi\ddot{q}(t) \rightarrow \ \ddot{q}(t) = \Phi^{\dagger}\ddot{x}(t) \tag{1}$$

If the modes can be sufficiently uncoupled, then the envelope of the modal signal for the *rth* mode can be described as a sum of the decaying harmonic function and its Hilbert transform as given by Equation 2.

$$Q_r(t) = q_r(t) + i\tilde{q}_r(t) \tag{2}$$

where $\tilde{q}_r(t)$ is the Hilbert transform of the signal and $Q_r(t) = A(t)\exp(i\psi(t))$. $A(t)$ denotes the magnitude of the envelope as given by $A(t) = \sqrt{q_r(t)^2 + \tilde{q}_r(t)^2}$ and $\psi(t)$ represents the instantaneous phase of the modal response as given by $\psi(t) = \tan^{-1}\left(\frac{\tilde{q}(t)}{q(t)}\right)$ [8]. Equation 2 is depicted in terms of modal displacement amplitude, but can also be applied to modal velocity and acceleration amplitude as governed by

$$|q_r| = \frac{|\dot{q}_r|}{\omega_r} = \frac{|\ddot{q}_r|}{\omega_r^2} \tag{3}$$

The objective is to describe the nonlinear damping and stiffness as a function of peak velocity amplitude such that type of nonlinearity can be described with the increase in amplitude. As a result, the instantaneous damped natural frequency can be described as the time derivative of the instantaneous phase and the instantaneous damping can be calculated from the time derivative of the amplitude as shown below

$$\omega_{r_{damped}} = \frac{d\psi(t)}{dt} \tag{4}$$

$$-\omega_r\zeta_r = \frac{dA(t)}{dt} \tag{5}$$

where ω_r is the natural frequency as governed by $\omega_r = \omega_{r_{damped}}/\sqrt{1-\zeta_r^2}$. However, given that experimental data yields discrete points, the data is fit with a spline with 50 points (knots). An in-depth discussion of the derivation of the Hilbert transform can be found in Feldman [9].

3. Experimental Methodology

The work presented in this paper was conducted on two C-shaped beams manufactured with Stainless Steel type ANSI 304. The two beams before and after assembly with two bolted connections at the ends are shown in Figure 3.1.

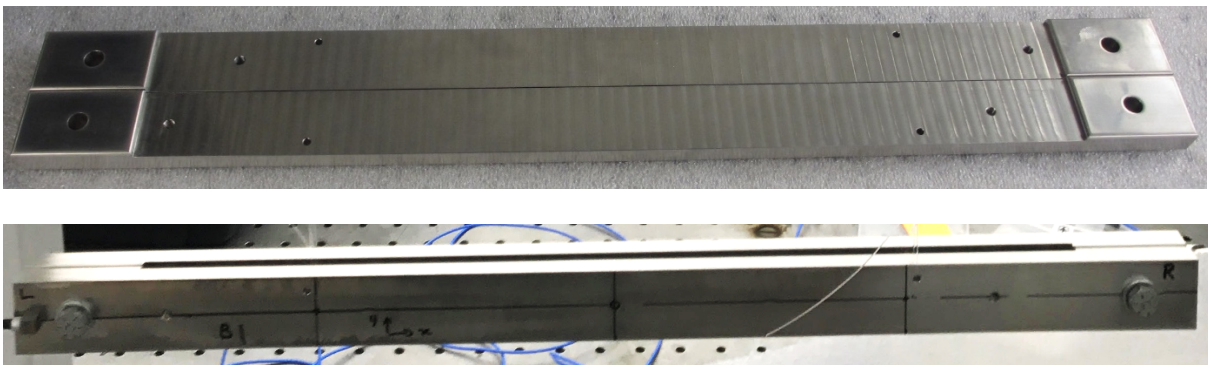

Figure 3.1: *Two separate beam halves of the S4 Beam (top) and the assembled beam (bottom)*

Each beam is 20 inches long, with two 2” x 1.25” contact surfaces. Each beam is 0.5” tall at the contact surface, and 0.38” elsewhere. All dimensions on the beam were manufactured with a 0.005” tolerance. Two different sets of beams were manufactured with variable surface conditions at the bolted interfaces: (1) convex interface with a center to edge drop of 0.005” to 0.008”, and (2) flat interface as shown below. All contact surfaces were polished to a minimum surface finish of Ra = 8.

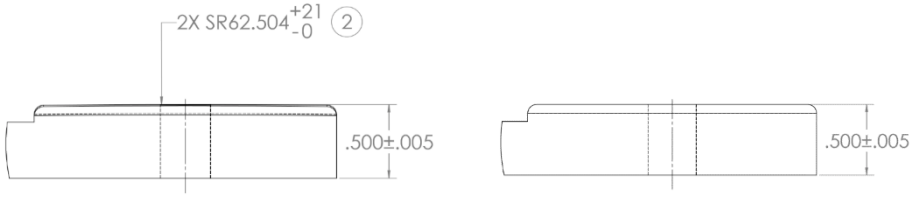

Figure 3.2: *Drawing of the convex (left) and flat (right) interfaces*

Prior to modal testing, four configurations of beams were assembled as indicated in Figure 3.3. B1-B2 features an interface of two convex surfaces in contact. This contact was modified slightly by placing thin stainless-steel washers at the interface for B1-B2W, in an effort to move the contact pressure distribution further away from the bolt holes. In B1-B6, the contact was such that a convex surface is mated with a flat surface. The flat-flat surface case is examined with B5-B6. All beams were assembled by 5/16"-24 bolts and nuts, and type – A washers.

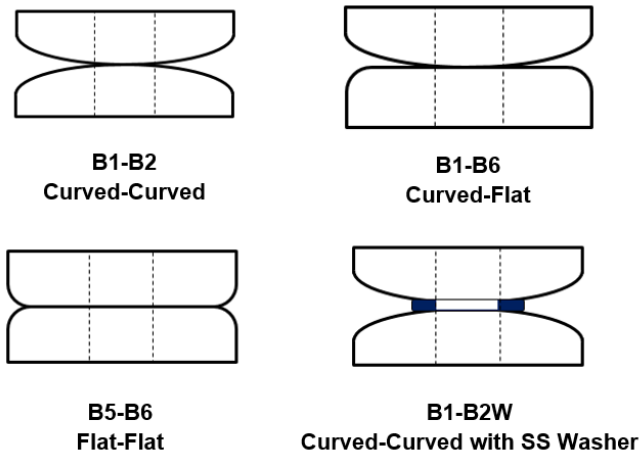

Figure 3.3: *Combinations of beams and their corresponding contact surfaces*

3.1 Impact Hammer Testing

Modal testing of the S4 Beam was accomplished by hanging the assembly using bungee cords and fishing line to emulate “free–free” boundary conditions with as little impact on the dynamics of the system as possible. Discrete points along the beams were excited by an impact hammer to obtain the linear mode shapes (at low impact amplitudes) and nonlinear time histories (at higher amplitudes) for the nonlinear system parameter identification. The bolted beams were tested at three torque levels: 10.2 N-m, 16.9 N-m, and 25.1 N-m to evaluate the effect of preload, and four input forces 10 N, 100 N, 250 N, and 500 N to assess the effect of input force on the joint nonlinearity. The experiment was then repeated for the four combinations of beams.

Prior to commencing testing at all torque and impact levels, the optimal setup was found to minimize the cable damping, and hence the number of accelerometers necessary to capture the desired mode shapes. This optimization process was carried out by progressively increasing the number of accelerometers and checking experimental natural frequencies and modal damping. Small variations with respect to a setup with a minimum number of accelerometers indicated that the added sensors did not significantly influence the structure. Cables were taped to the beam, as it was found that it mitigated additional damping to the system in these conditions. In this phase, prior to nonlinear data collection, the interest was not in the mode shapes, but rather in the natural frequencies and damping ratios, so that the setup with a minimum number of sensors was used as a reference to evaluate structural effects (mass and damping) of the accelerometers on the beam.

The first six elastic mode shapes for B1-B2 are reported in Figure 3.4 and were considered the target modes when defining the accelerometer placement.

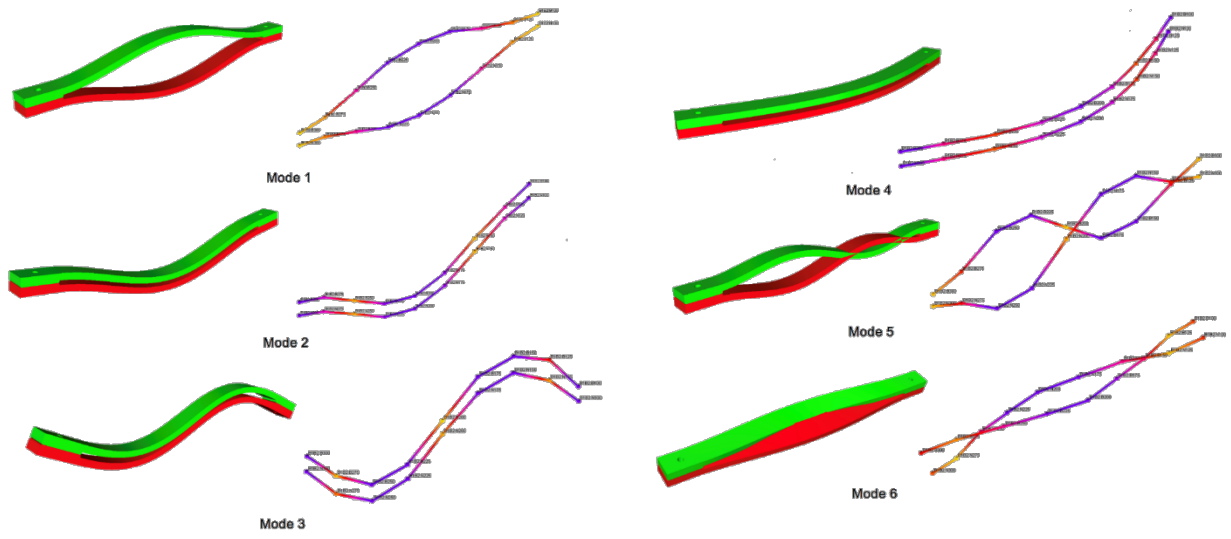

Figure 3.4: *Linear elastic mode shapes of the S4 Beam*

Figure 3.5 depicts the optimal sensor setup for B1-B2, which was then replicated for the three other combinations.

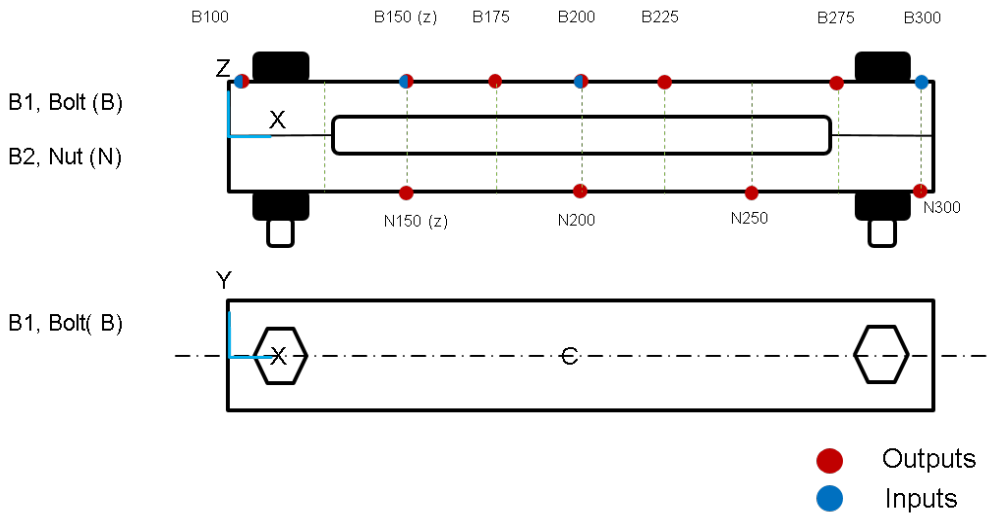

Figure 3.5: *Optimal test setup*

Accelerometer locations were chosen to obtain completely observable modes in the bandwidth of interest. Input locations were similarly selected such that for each mode there was at least one point efficiently exciting the mode. As a result, the final setup consisted of ten accelerometers, with nine tri-axial and one uniaxial, for a total of 28 output channels. Additional optimization was done using a roving hammer test to evaluate the ideal input locations as depicted in Appendix A. To capture the first six elastic modes, the test bandwidth was limited to 800 Hz based on the preliminary modal simulation of the finite element model. The data acquisition was performed by Siemens LMS Test Lab and LMS SCADAS system.

3.2 Joint Profile Testing

In order to capture the change in the joint characteristics due to the change in torque, the two contact areas of the beams were characterized with normal contact pressure measurements using Fujifilm Prescale pressure films. Three film types were used to capture different pressure ranges for all torque levels as depicted in Table 3.1. The films were placed between the two contacting surfaces as the beams were fastened with two bolts up to the prescribed torque level. Following the preload, the beams were held together for two minutes before loosening the bolts and removing the pressure film. The experiment was repeated for all three torque levels and all beam sets.

Table 3.1: *Film types and corresponding pressure ranges*

Film type	Pressure Range [MPa]
Low	2.41 – 9.65
Medium	9.65 – 48.95
High	48.95 – 127.55

4. Experimental Results

Three types of data were collected during the experiments: (1) joint pressure distributions, (2) frequency response functions (FRFs), and (3) time histories. The pressure film results were used to qualify the influence of the pre-stress on the joint interface due to the torque. The FRFs were used to determine the linear mode shapes and linear modal parameters, whereas the time histories were used to determine the nonlinear characteristics of the beam. For the subsequent

discussion, beam sets B1-B2 and B5-B6 were mainly analyzed with respect to pressure distribution, torque level, and impact level.

4.1 Interface Characterization

The pressure film measurements of the three torque cases for different contact surface combinations are summarized below in Figures 4.1 to 4.3. The B1-B2 (convex-convex) case had a high concentration of pressure at the proximity of the through hole and showed small changes in pressure areas across the film due to the change in torque levels. As an intermediate between a spherical interface and a flat interface, the B1-B6 (convex-flat) case was similar to the previous case with a concentration of pressure near the hole, but with a larger contact area. In contrast, the B5-B6 (flat-flat) case showed a significant amount of pressure saturation with low to medium pressure readings across most of the film. This suggests that the B1-B2 (convex-convex) should have the smallest contact area, whereas B5-B6 (flat-flat) should have the largest. The pressure readings and contact area decreased for all contact surface combinations as the value of the preload torque was decreased on the joint. It is worth pointing out that the B5-B6 (flat-flat) showed the most dramatic reduction in pressure readings compared to the other cases.

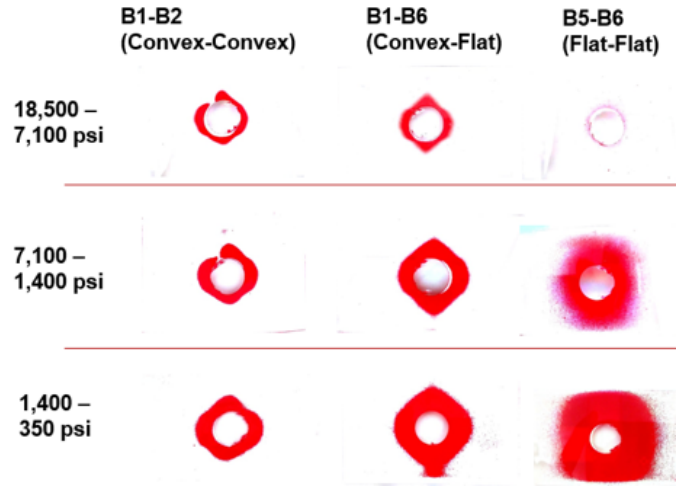

Figure 4.1: *Pressure film measurement at 25.1 N-m torque*

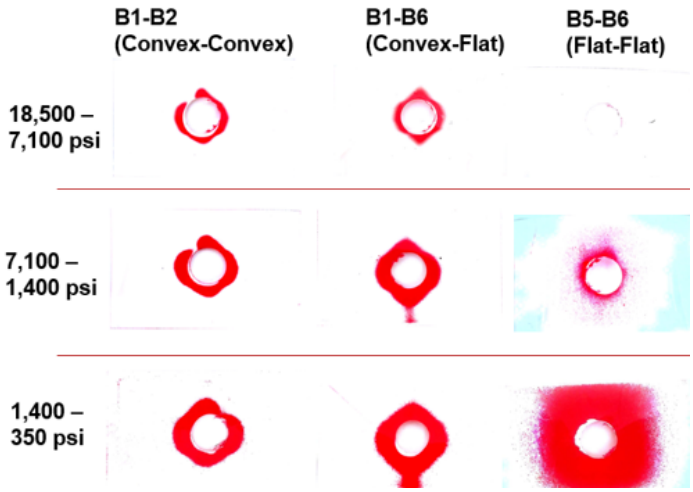

Figure 4.2: *Pressure film measurement at 16.9 N-m torque*

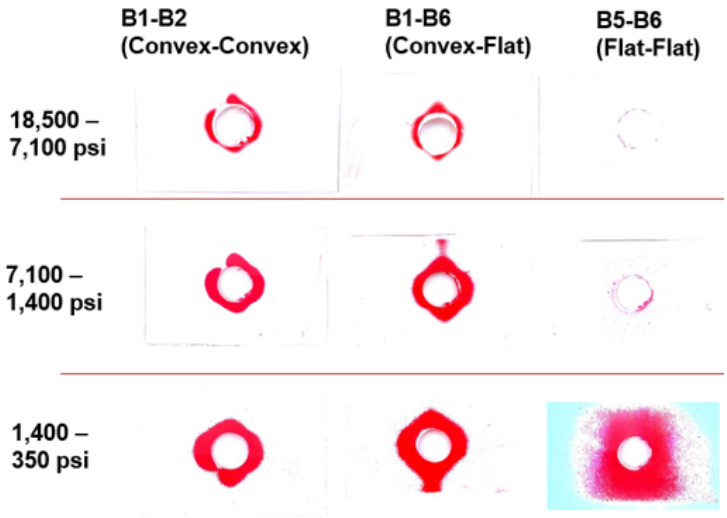

Figure 4.3: *Pressure film measurement at 10.2 N-m torque*

To understand the correlation between the pressure readings across the joint and the structural response of the assembly, the change in the linear natural frequency with respect to varying torque levels was examined for the three contact surface combinations. Table 4.1 summarizes the linear natural frequency of the first six modes for the three contact surface combinations at varying torque levels.

Table 4.1: *Linear natural frequencies (Hz) of the assembly vs bolt torque*

Mode #	B1-B2 (convex-convex)			B1-B6 (convex-flat)			B5-B6 (flat-flat)			Mode Description
	10.2 [N-m]	16.9 [N-m]	25.1 [N-m]	10.2 [N-m]	16.9 [N-m]	25.1 [N-m]	10.2 [N-m]	16.9 [N-m]	25.1 [N-m]	
1	235.2	237.3	239.7	233.9	237.8	240.3	253	256.4	258.6	1st out of phase bending - Z
2	327.8	328.5	329.1	326.4	327.3	327.8	330.3	331	331.8	1st in phase bending - Z
3	483.7	483.7	483.7	481.6	481.6	481.8	478.7	478.5	478.5	2nd in phase bending - Z
4	570.5	570.6	570.7	568.8	568.7	569.3	568	567.6	567.4	1st in phase bending - Y
5	641.4	647.1	653.6	638.1	648.2	655.4	693.2	703.5	710	2nd – out of phase bending - Z
6	655.6	672.2	686.5	655	682.2	696.8	823.4	841.4	854.8	1st – out of phase bending - Y

Modes 2, 3, and 4 show similar linear natural frequency values for any torque level or contact surface combination, concluding that the stiffness of these modes is not affected by the joint. Since the ends of the beams deflect parallel to each other at the joints, the influence of the joint characteristics to the structural response of the assembly due to varying contact conditions is mitigated. However, Mode 2 is a possible exception to this rule, since bending in this shape induces a shear stress onto the bolted interfaces.

In contrast, for the mode shapes with tensile loads or breathing of the joint, and with shearing of joints (Modes 1, 5, and 6), the structural response of the assembly demonstrated a strong

correlation to the varying joint characteristics. Figure 4.4 shows the plot of the natural frequencies of Modes 1 and 5 as the torque is varied. It seems reasonable that both of these modes show identical trends since they have tensile loads at the joints and exhibit joint breathing. In addition, for a constant torque level, Mode 6 for the flat – flat configuration (B5-B6) depicts a frequency shift of ~150 Hz in comparison to B1-B2 as a result of the flat interface.

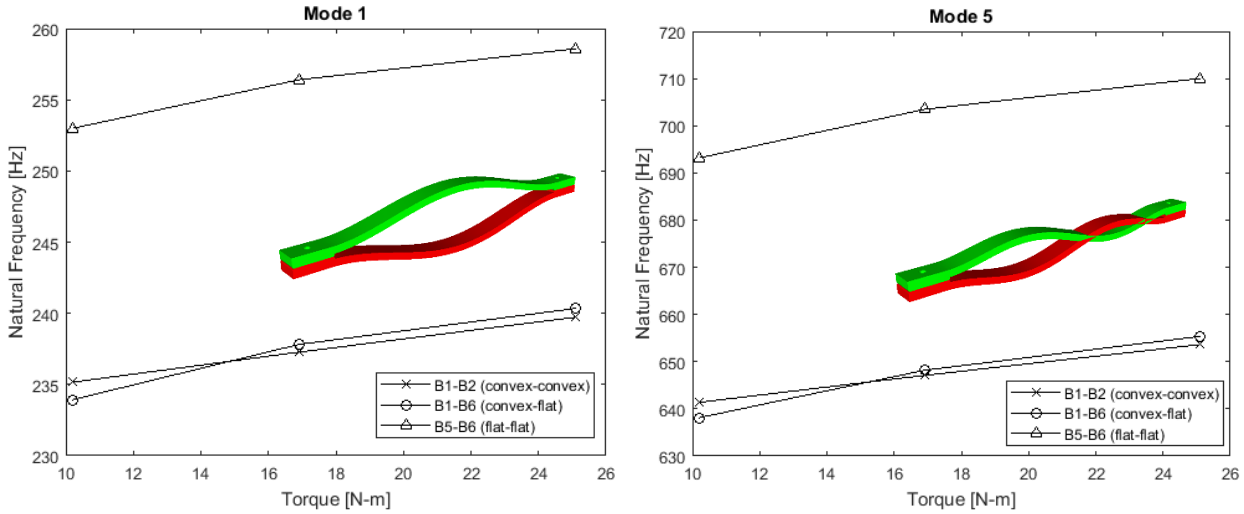

Figure 4.4: *Linear natural frequency of Modes 1 (left) and Mode 5 (right)*

These observations follow the results of the pressure film measurements in Figures 4.1-4.3, where B5-B6 (flat-flat) case has a larger contact area at all torque levels compared to the other two cases. At 10.2 N-m torque, B1-B2 (convex-convex) case shows a similar contact area to the B1-B6 (convex- flat) case, but a higher pressure reading since the pressure is concentrated near the bolt, resulting in stiffer joint. As the torque is increased, the contact area of the B1-B6 (convex-flat) case exceeds the B1-B2 (convex-convex) case, and therefore a higher stiffness at these torque levels. It is also interesting to note that the natural frequency is measurably sensitive to the bolt torque even for B1-B2 and B1-B6, even though the contact pressure distributions shown previously suggested that the contact area changed very little for these structures.

Figure 4.5 shows the case of Mode 6, which involves rotational shearing at the joints. Mode 6 follows an almost identical trend to the previous comparison where the B5-B6 (flat-flat) case has a significantly higher natural frequency across the torque level compared to the other contact surface combinations and B1-B6 (convex-flat) has a higher natural frequency at 16.9 N-m and 25.1 N-m torque levels.

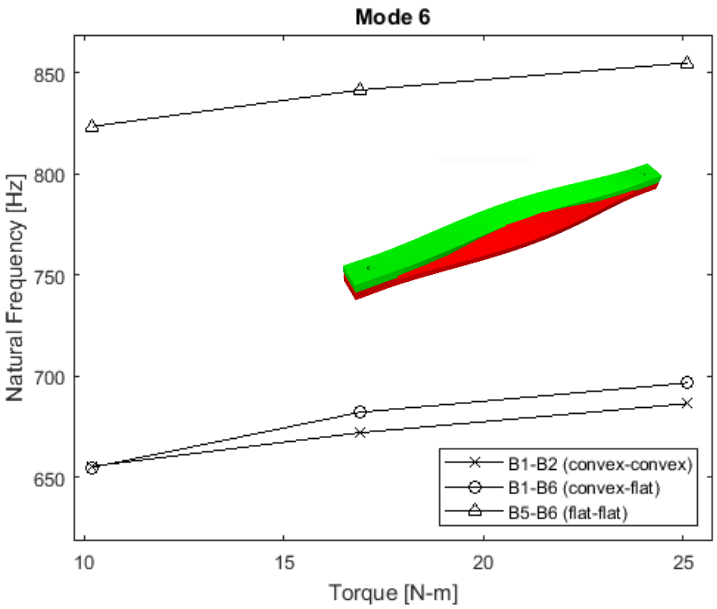

Figure 4.5: *Linear natural frequency of Mode 6*

To evaluate the repeatability and accuracy of the linear analysis, the most linear case where the structure is assembled with the largest torque (25.1 Nm) and impacted at the lowest excitation level is examined. A larger torque should produce less slipping along the contact interface, therefore less friction and nonlinearity. The linear resonance frequencies for the two extreme configurations (convex–convex, flat–flat), are depicted below in Table 4.2 with the percent variation from the average value for the natural frequency. The variation in frequency was computed through multiple measurements to ensure that the beam had repeatable results within a single test setup.

Table 4.2: *Natural frequencies (Hz) and percent variation at a 25.1 Nm torque*

Mode	B1-B2	B5-B6
1	239.1 (+1.92%)	258.0 (+1.98%)
2	328.6 (0.34%)	331.7 (+0.42%)
3	483.5 (-0.02%)	478.5 (-0.04%)
4	570.7 (+0.05%)	567.7 (-0.05%)
5	652.4 (+1.94%)	708.3 (+2.16%)
6	683.8 (+4.73%)	851.8 (+3.14%)

Though the repeatability resulted in frequency disparities, all remained within 5% variance. Next, the Hilbert transform can be used on the decoupled modes to identify the nonlinearities in select modes.

4.2 Nonlinearity Detection and Analysis

FRFs are used to qualitatively determine which modes exhibited nonlinearity. To do this, the FRFs were compared between each beam combination and between different torque levels and different force amplitudes. This comparison is only qualitative, since the amplitude-varying, and hence time varying modal properties are all convolved into a single FRF. In the following subsection, the time histories will be used to quantitatively identify the nonlinearities in those modes that exhibited significant nonlinearity. Within the first six linear elastic modes, three modes

of interest were chosen based on the behavior of the joint as well as the degree of nonlinearity in response to a larger excitation. Figure 4.6 depicts the cumulative summation of all FRFs for the four levels of excitation at the middle torque level (16.9 Nm) for the B1-B2 (convex-convex) beam, and Figure 4.7 shows the results for the B5-B6 (flat-flat) beam.

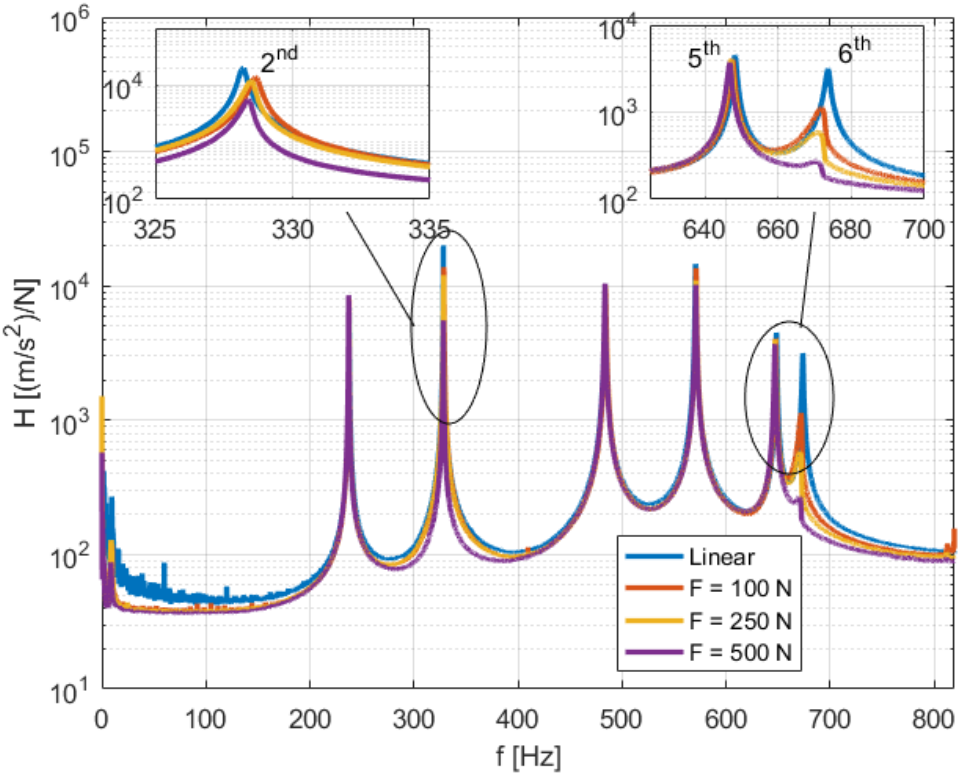

Figure 4.6: *Amplitude and force variation for B1-B2 for 16.9 Nm Torque*

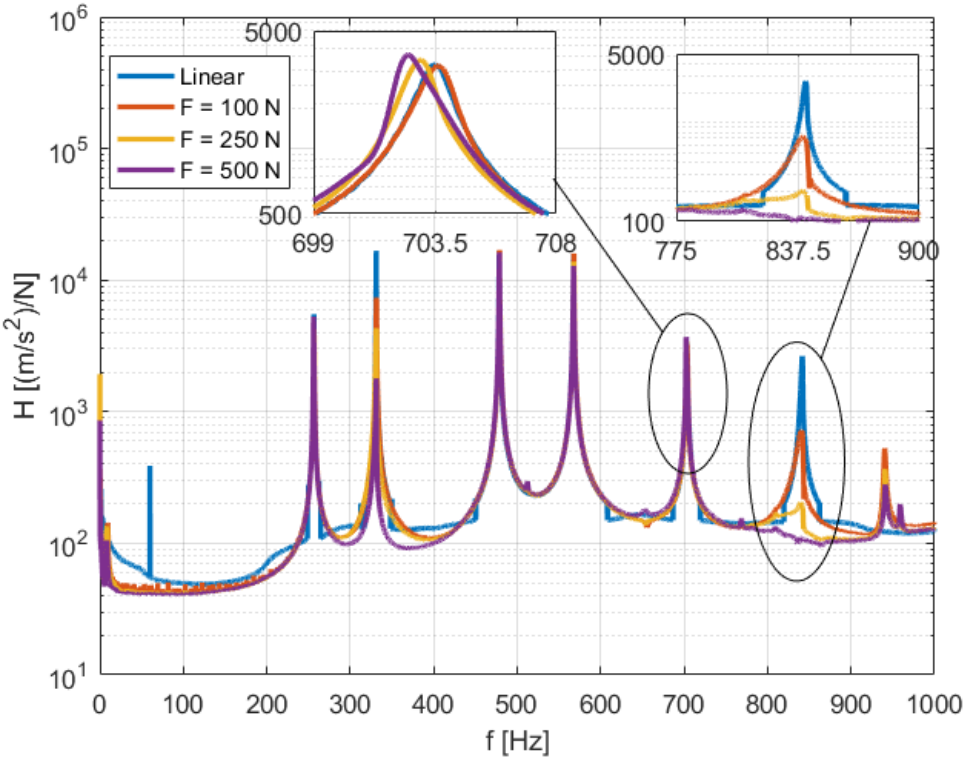

Figure 4.7: *Amplitude and force variation for B5-B6 for 16.9 Nm Torque*

As evident by both beam configurations, mode six exhibits a large degree of damping nonlinearity as depicted by the widening of the peak and drop in amplitude. Therefore, it is a mode of interest to identify this damping nonlinearity using the Hilbert transform algorithm. To help explain why each mode does or does not exhibit significant nonlinearity, Table 4.3 describes the effect that each mode shape is expected to have on the joint.

Table 4.3: *Beam motion and joint behavior*

Mode	Description	Joint Behavior
1	1st out of phase bending - Z	Opening/closing of the joint
2	1st in phase bending - Z	Shearing of the joint
3	2nd in phase bending - Z	None
4	1st in phase bending - Y	None
5	2nd – out of phase bending - Z	Opening/closing of the joint
6	1st – out of phase bending - Y	Rotational shearing of the joint

The Hilbert transform analysis results for the fundamental mode of the system are presented in Appendix B. It exhibits the breathing of the joint which results in a weak stiffness nonlinearity, with no significant change in damping due to micro-slip. The results in Appendix B show erratic behavior of the damping, but it is important to note that the changes are small and are probably dominated by uncertainty in the Hilbert transform analysis.

Modes 2 and 6 are further analyzed in this section since both modes produce shearing at the joint and hence produce damping nonlinearity. Therefore, to evaluate the degree of nonlinearity of each mode with respect to the lowest torque, the Hilbert transform was used to find the damping and frequency variation as a function of peak velocity amplitude. The frequency variation is depicted as a percent change from the linear natural frequency. Prior to examining additional

trends for torque, impact, and configuration of the beams, the results for mode six are depicted in detail in Figures 4.8 and 4.9 for the two different configurations at the lowest torque. Given that multiple points can efficiently excite each mode, as detailed in Appendix A, these results are based on the analysis of the data at B200Y, the center of the beam. The horizontal axis in each of these plots is the peak amplitude, here defined as the amplitude at the point on the beam that has the largest motion for the mode of interest. In each response, the system is expected to behave linearly, although the measured signals become noisy at very low amplitudes leading to spurious oscillations in the measurements. At higher amplitudes the nonlinearity is evident.

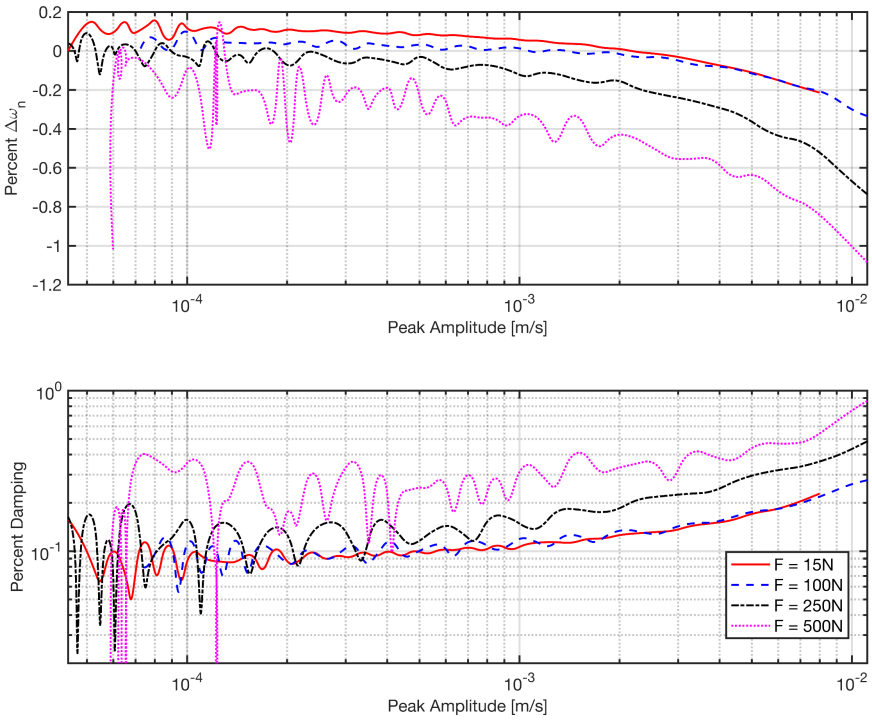

Figure 4.8: *Natural frequency and damping versus amplitude for Mode 6 at 10.2 Nm torque for B1-B2 using B200Y as the drive point*

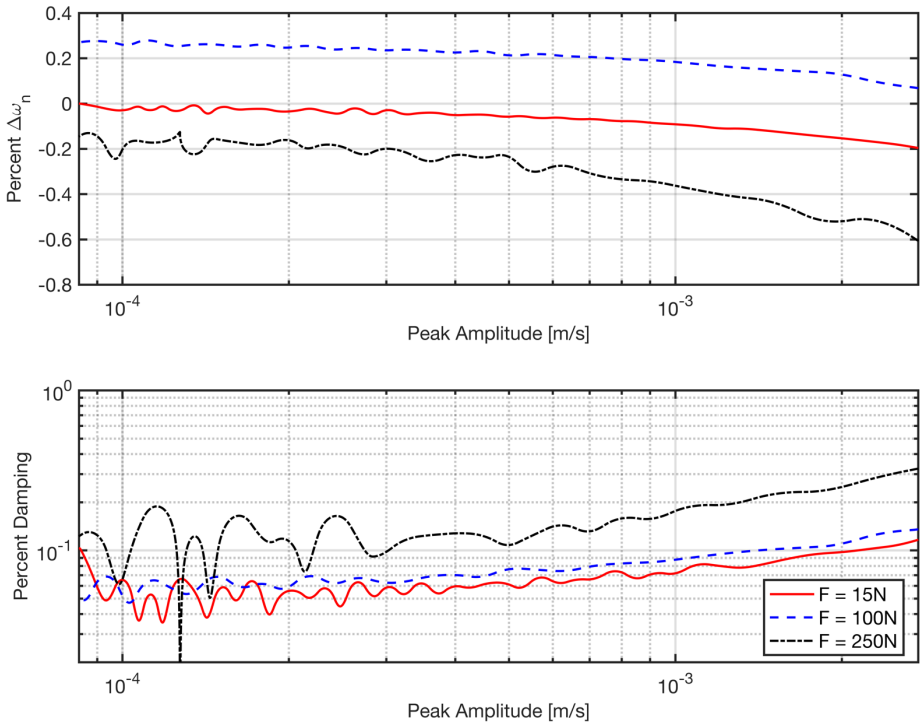

Figure 4.9: *Natural frequency and damping versus amplitude for Mode 6 at 10.2 Nm torque for B5-B6 using B200Y as the drive point*

The results show that B5-B6 did not always return to the same linear natural frequency when larger forces were applied. This suggests that some change has occurred at the interface due to the vibration, and potentially calls the measurements into question. This is surprising because the joints were "broken in" prior to the tests by tapping the beam many times with a rubber mallet. No result is shown for mode six at an impulse of 500 N for B5-B6. This is because the mode became so heavily damped that Hilbert transform analysis was no longer possible. The smoothness of the damping versus amplitude curves at low force levels suggests that the nonlinearity is weak and the joints are in a state of micro-slip. However, at greater excitation levels the modal behavior does not follow the same trend, suggesting either that macro-slip has occurred or that this mode has become coupled to other modes in the structure. The remainder of the analysis presented below shows only those cases that seem to be dominated by micro-slip, because only those cases have the weak modal coupling necessary for the Hilbert transform analysis to be valid.

The following four figures examine modes two and six for both configurations of beams at various drive points. A single drive point is capable of exciting multiple modes, which can then induce additional modal coupling. However, the results in [5] suggest that the curve with the lowest damping should be a good estimate for the damping due to that mode alone. Table 4.4 gives the drive points used for each mode in this analysis.

Table 4.4: *Drive point used for each mode*

Mode	Drive Point	Description
2	B100 – Z	Left end of beam
	B200 – Z	Center of beam
	B300 – Z	Right end of beam
6	B100 – Y	Left end of beam
	B200 – Y	Center of beam

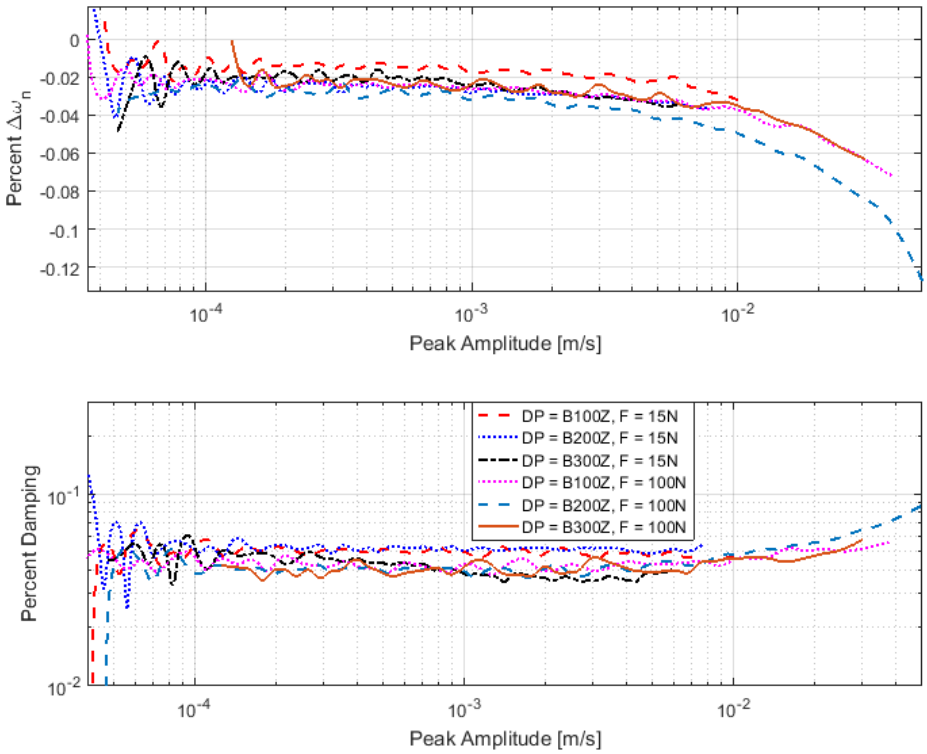

Figure 4.10: *Natural Frequency and damping versus amplitude for Mode 2 at 10.2 Nm torque for B1-B2*

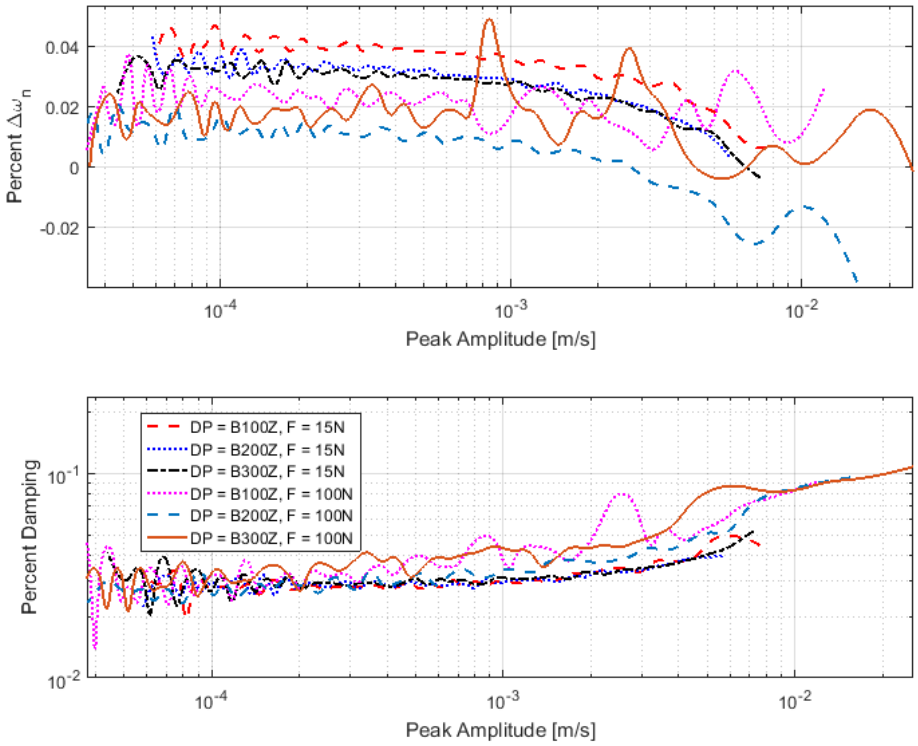

Figure 4.11: *Nat. Freq. and Damping versus amplitude for Mode 2 at 10.2 Nm torque for B5-B6*

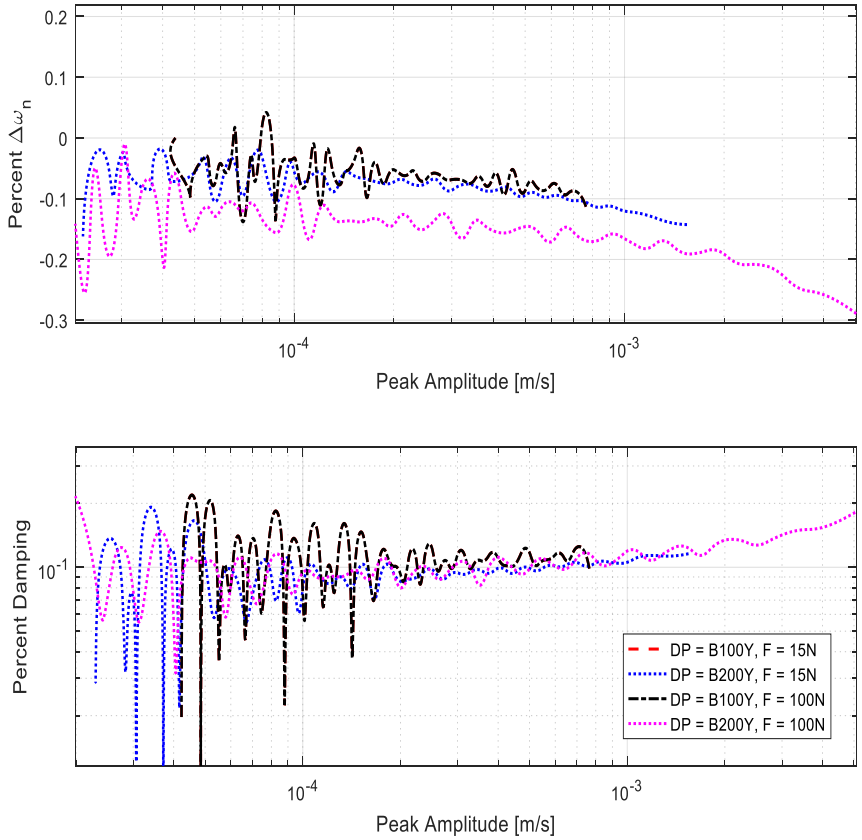

Figure 4.12: Nat. Freq. and Damping versus amplitude for *Mode 6 at 10.2 Nm torque for B1-B2*

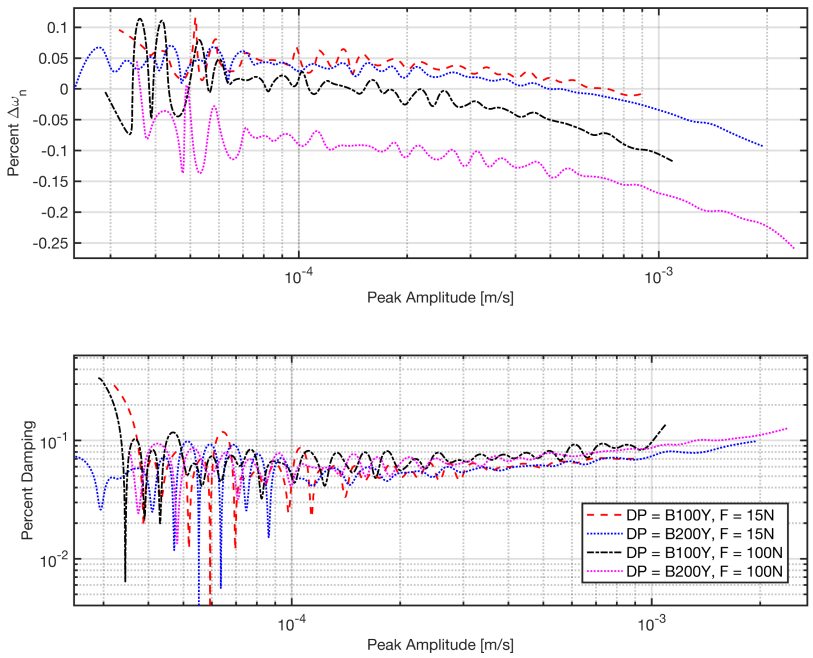

Figure 4.13: Nat. Freq. and Damping versus amplitude for *Mode 6 at 10.2 Nm torque for B5-B6*

Neglecting the scatter in the data at low amplitudes, the different drive points produced relatively similar trends. For modeling purposes, the results of the center drive point, B200-Z and B200–Y should be used for both modes for both configurations. The other drive points either do not excite the beam well or introduce additional modal coupling. To understand the percent variation of the damping and frequency, Table 4.5 depicts the maximum deviation for the two modes of interest.

Table 4.5: *Maximum deviation as a function of amplitude for 10.2 Nm torque*

Beam	Mode	Max Frequency Change	Max Damping Change	Type of Nonlinearity
B1-B2	2	-0.14%	148%	Damping NL
	6	-0.33%	582%	Damping NL
B5-B6	2	-0.08%	95%	Damping NL
	6	-0.26%	316%[1]	Damping NL

In both cases for mode six, the percent damping of the mode increased extensively, depicting a large damping nonlinearity for the mode with much smaller stiffness nonlinearity. In addition, the force varying Hilbert transform curves for mode six for the largest torque (25.1 Nm) are also shown below.

[1] Note that the shift for B5-B6 is in response to a 250N excitation, rather than a 500 N excitation as with B1-B2, given that the mode was not able to be modally filtered due to the significant nonlinearity

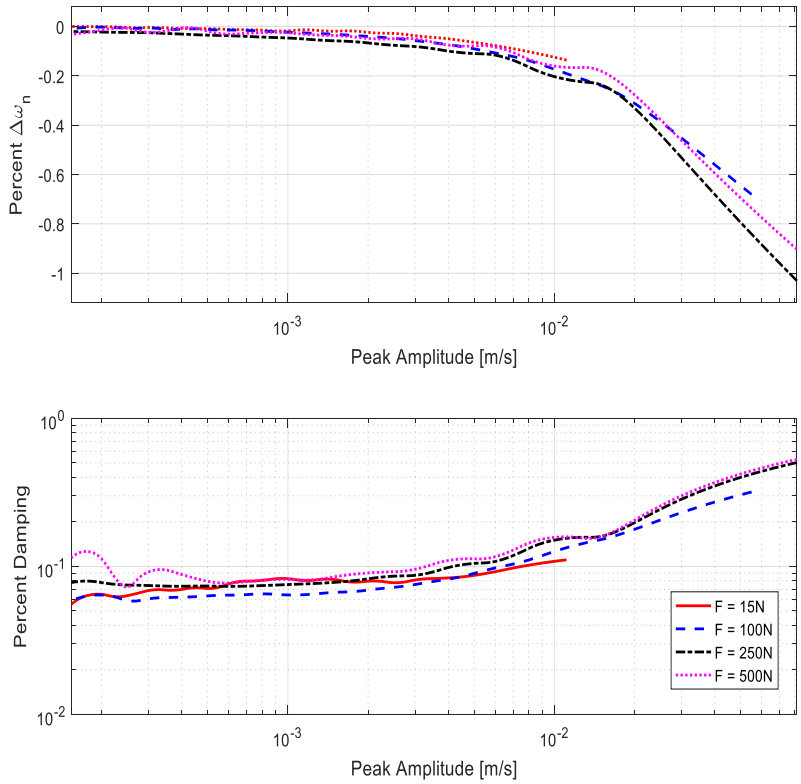

Figure 4.14: Nat. freq. and damping versus amplitude for *Mode 6 at 25.1 Nm torque for B1-B2*

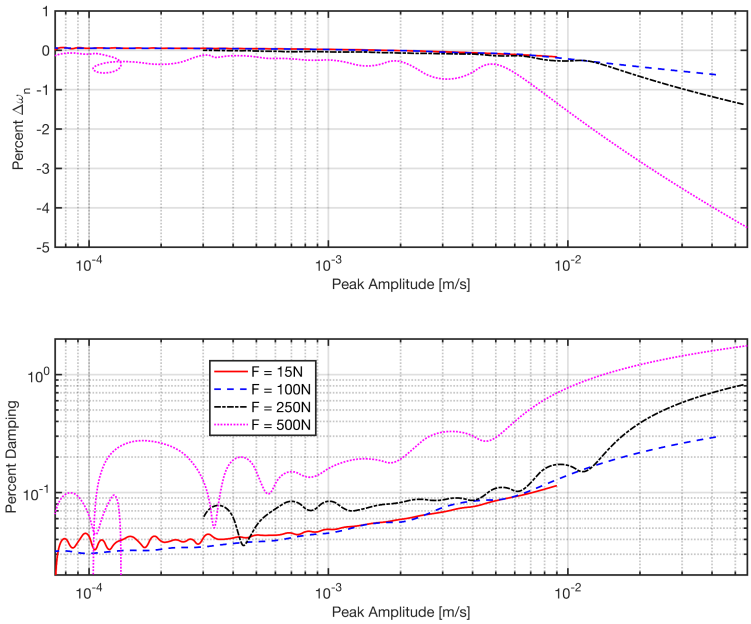

Figure 4.15: Nat. freq. and damping versus amplitude for *Mode 6 at 25.1 Nm torque for B5-B6*

Even at the largest torque with the stiffest joint, mode six exhibits large stiffness and damping

nonlinearities. At 500N, mode six seems to exhibit macro-slip as seen by the erratic deviating trend from the other impulse levels, and so that data should be used appropriately.

In an effort to classify the linearity of the four configurations, the variance of frequency and damping for each beam set was analyzed at an intermediate force (100 N) and both the lowest and highest torque to lightly excite the nonlinearity. Figure 4.16 depicts the results of this comparison.

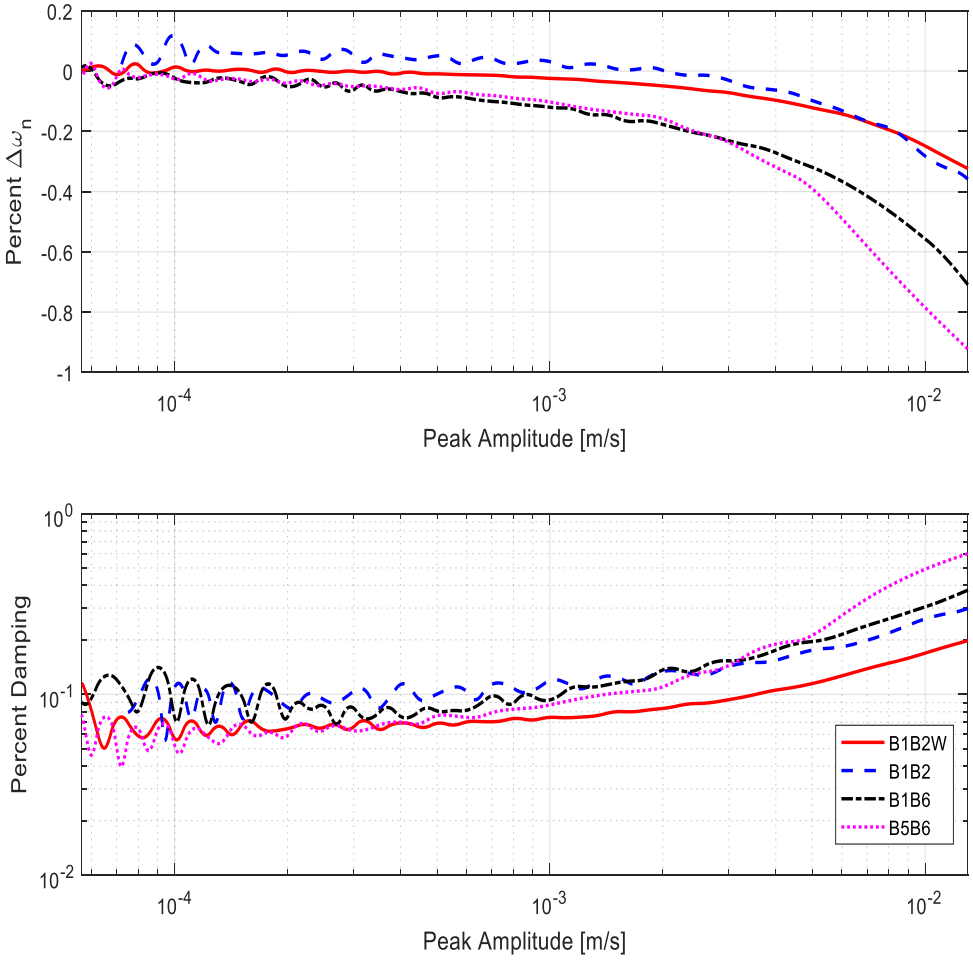

Figure 4.16: *Comparison of frequency and damping across the different beam combinations for an intermediate force level and the lowest torque*

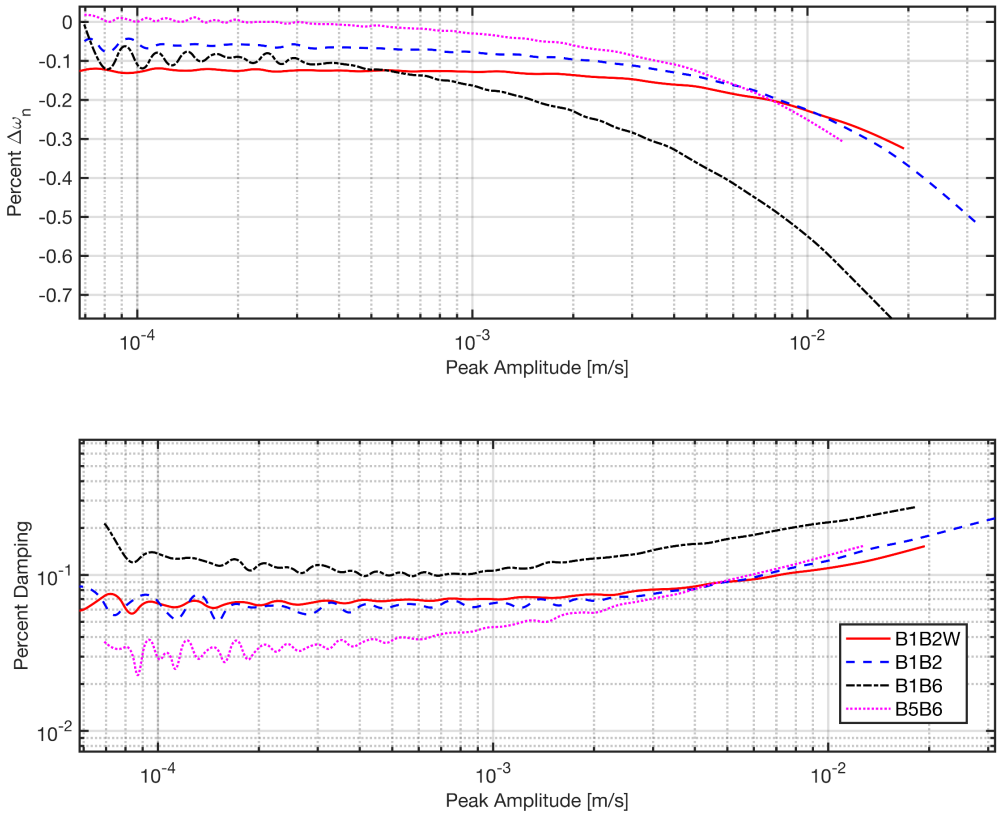

Figure 4.17: *Comparison of frequency and damping across the different beam combinations for an intermediate force level and the highest torque*

Between the four beam sets, the convex beam set and the convex – flat set are classified in the same "family" due to similar modal frequencies, whereas the other two sets are in the same "family" of beams. The washer configuration and flat–flat configuration had similar resonant frequencies, whereas the convex–flat and convex beams had similar resonances. In terms of damping for the lowest torque, the beams can be classified from relatively linear to significantly nonlinear based on the damping variance as given: (1) convex–convex with washer (B1-B2W), (2) convex–convex (B1-B2), (3) convex–flat (B1-B6), and (4) flat–flat (B5-B6). However, at the higher torque, the beams show variable trends with respect damping, yielding it difficult to classify the beams. Even though the slip is restricted at the higher torque, the pressure in the contact surface increases, requiring the same energy dissipation as with lower torque; therefore, additional torque does little to impact the nonlinearity in the joint.

5. Conclusion

This work sought to characterize a new benchmark structure and to provide a rich data set against which simulations may be compared when seeking to predict damping nonlinearities. The S4 beam, consisting of two C beams bolted together at the ends, was tested and the first six elastic modes, all below 800 Hz were characterized both linearly and nonlinearly. The pressure distributions were characterized and qualitatively correlated to variations in the linear natural frequencies and in the nonlinearity observed. As in other studies, those modes that exhibited shearing of the joint yielded as the strongest nonlinearity with respect to damping. In general,

none of the modes showed large stiffness nonlinearities even though the damping of some modes changed by a factor of five or more.

Between the four configurations of beams, the beams that had flat interfaces depicted the largest damping nonlinearity with a 316% increase in damping for the second largest impact excitation level, the highest that could be reliably characterized. On the other hand, the curved beams with a washer depicted the least damping nonlinearity.

Although the testing was judged successful, throughout the process of nonlinear model identification, some lessons were learned that could improve the results in future testing. Most importantly, the sample rate chosen was barely adequate, and while the LMS system was not able to take longer time records in FFT mode, throughput mode should have been used so that the modal hammer impacts could be captured more accurately and then it might have been possible to use alternate identification methods such as the Restoring Force Surface Method as an additional method to characterize the joint [7]. Furthermore, a shaker or automatic hammer could provide additional accuracy when compared to a modal hammer. Lastly, it was sometimes noted that if the modal filtered response was not a SDOF system with a single mode, the results of the Hilbert transform for frequency and damping were erratic, impeding the proper fit of the data. Perhaps the modal filter used for this system could have been improved by testing at even lower levels than was used here (i.e. perhaps using higher sensitivity sensors) to extract the mode shapes more accurately.

In any event, this beam provides a significant data set that can now be used to validate numerical predictions of damping. Given that the beam exhibits modes with all degrees of damping nonlinearities, the beam should provide a good test case for numerical methods.

Acknowledgements

This research was conducted at the 2017 Nonlinear Mechanics and Dynamics (NOMAD) Research Institute supported by Sandia National Laboratories. Sandia National Laboratories is a multi-mission laboratory managed and operated by National Technology and Engineering Solutions of Sandia, LLC., a wholly owned subsidiary of Honeywell International, Inc., for the U.S. Department of Energy's National Nuclear Security Administration under contract DE-NA-0003525.

Works Cited

[1] D. R. Roettgen and M. S. Allen, "Nonlinear characterization of a bolted, industrial structure using a modal framework," *Mechanical Systems and Signal Processing,* 2016.

[2] B. J. Deaner, M. S. Allen, M. J. Starr , D. J. Segalman and H. Sumali, "Application of Viscous and Iwan Modal Damping Models to Experimental Measurements From Bolted Structures," *ASME Journal of Vibrations and Acoustics,,* vol. 137, p. 12, 2015.

[3] M. S. Allen, R. Lacayo and M. R. W. Brake, "Quasi-static Modal Analysis based on Implicit Condensation for Structures with Nonlinear Joints," in *ISMA*, Leuven, Belgium, 2016.

[4] H. Festjens, G. Chevallier and J.-L. Dion, "A numerical tool for the design of assembled structures under dynamic loads," *International Journal of Mechanical Sciences,* vol. 75, pp. 170 - 177, 2013.

[5] M. S. Bonney, B. A. Robertson, F. Schempp, M. Mignolet and M. R. Brake, "Experimental Determination of Frictional Interface Models," in *Dynamics of Coupled Structures - Proceedings of the 34th IMAC*, New York, 2016.

[6] T. Dossogne, "Experimental Assessment of the Influence of Interface Geometries on Structural Dynamic Response In: Allen M., Mayes R., Rixen D. (eds) Dynamics of Coupled Structures," in *Conference Proceedings of the Society for Experimental Mechanics Series*, 2017.

[7] G. Kerschen, K. Worden, A. F. Vakakis and J. -. C. Govindal, "Past, present and future of nonlinear system identification in structural dynamics," *Mechanical Systems and Signal Processing,* vol. 20, pp. 505-592, 2006.

[8] R. M. Lacayo, B. J. Deaner and M. S. Allen, "A numerical study on the limitations of modal Iwan models for impulsive excitations," *Journal of Sound and Vibration,* vol. 390, pp. 118-140, 3 March 2017.

[9] M. Feldman, "Non-linear system vibration analysis using Hilbert transform--I. Free vibration analysis method'Freevib'," *Mechanical Systems and Signal Processing,* vol. 8, no. 2, pp. 119-128, 1994.

[10] A. Majumdar and B. Bhushan, "Role of fractal geometry in roughness characterization and contact mechanics of surfaces," *Journal of Tribology,* vol. 112, no. 2, pp. 205-216, 1990.

[11] Y. Zhao, C. Yang, L. Cai, W. Shi and Y. Hong, "Stiffness and Damping Model of Bolted Joints and Uneven Surface Contact Pressure Distribution," *Journal of Mechanical Engineering,* vol. 62, no. 11, pp. 665-677, 2016.

6. Appendix A

Test Setup

For modal data acquisition, two beams were bolted together and a set of points was identified along the two beams, naming B the beam with the bolt and N the beam with the nut. Points were numbered from 100 to 300, 100 as the extremity close to the origin and 300 the other end of the beams. A point every 25 units is defined, for both beams. Table A.1 reports the coordinate of each point.

Table A.1: *Testing points names and locations*

Name	x [m]	y [m]	z [m]		Name	x [m]	y [m]	z [m]
B100	0.0125	0.0000	0.0111		**N100**	0.0125	0.0000	-0.0111
B125	0.0635	0.0000	0.0111		**N125**	0.0635	0.0000	-0.0111
B150	0.1270	0.0000	0.0111		**N150**	0.1270	0.0000	-0.0111
B175	0.1905	0.0000	0.0111		**N175**	0.1905	0.0000	-0.0111
B200	0.2540	0.0000	0.0111		**N200**	0.2540	0.0000	-0.0111
B225	0.3175	0.0000	0.0111		**N225**	0.3175	0.0000	-0.0111
B250	0.3810	0.0000	0.0111		**N250**	0.3810	0.0000	-0.0111
B275	0.4445	0.0000	0.0111		**N275**	0.4445	0.0000	-0.0111

B300	0.4955	0.0000	0.0111		**N300**	0.4955	0.0000	-0.0111

Optimal Input Location

To define the location of each accelerometer and to select the input point, Table A.1 was constructed using the amplitude of the linear mode shapes as a basis from the roving hammer test, with the modes of interest highlighted. It reports the amplitude of motion of each mode at each of the point, using a 0-3 scale with 0 not affecting the mode, and 3 having the largest effect.

Table A.1: *Points amplitude scale for each mode*

Mode	**B100**	**N100**	**B125**	**N125**	**B150**	**N150**	**B175**	**N175**	**B200**
1	0	0	0	0	1	1	2	2	3
2	3	3	2	2	0	0	2	2	3
3	3	3	0	0	3	3	3	3	0
4	3	3	1	1	0	0	2	2	3
5	0	0	1	1	3	3	3	3	0
6	1	1	0	0	1	1	2	2	3
7	1	1	2	2	3	3	2	2	0
8	0	0	2	2	3	3	0	0	3
9	2	2	0	0	0	3	0	0	3
10	3	3	3	3	0	0	3	3	0
Mode	**N200**	**B225**	**N225**	**B250**	**N250**	**B275**	**N275**	**B300**	**N300**
1	3	2	2	1	1	0	0	0	0
2	3	2	2	0	0	2	2	3	3
3	0	3	3	3	3	0	0	3	3
4	3	2	2	0	0	1	1	3	3
5	0	3	3	3	3	1	1	0	0
6	3	2	2	1	1	0	0	1	1
7	0	2	2	3	3	2	2	1	1
8	3	0	0	3	3	2	2	0	0
9	3	0	0	3	3	0	0	2	2
10	0	3	3	0	0	3	3	3	3

The table allowed to easily identify, from a qualitative point of view, modal nodes and to define inputs and outputs suitable to excite and collect information about all the first 6 modes (additional modes 7 to 10 reported).

7. Appendix B

Mode 1 Results

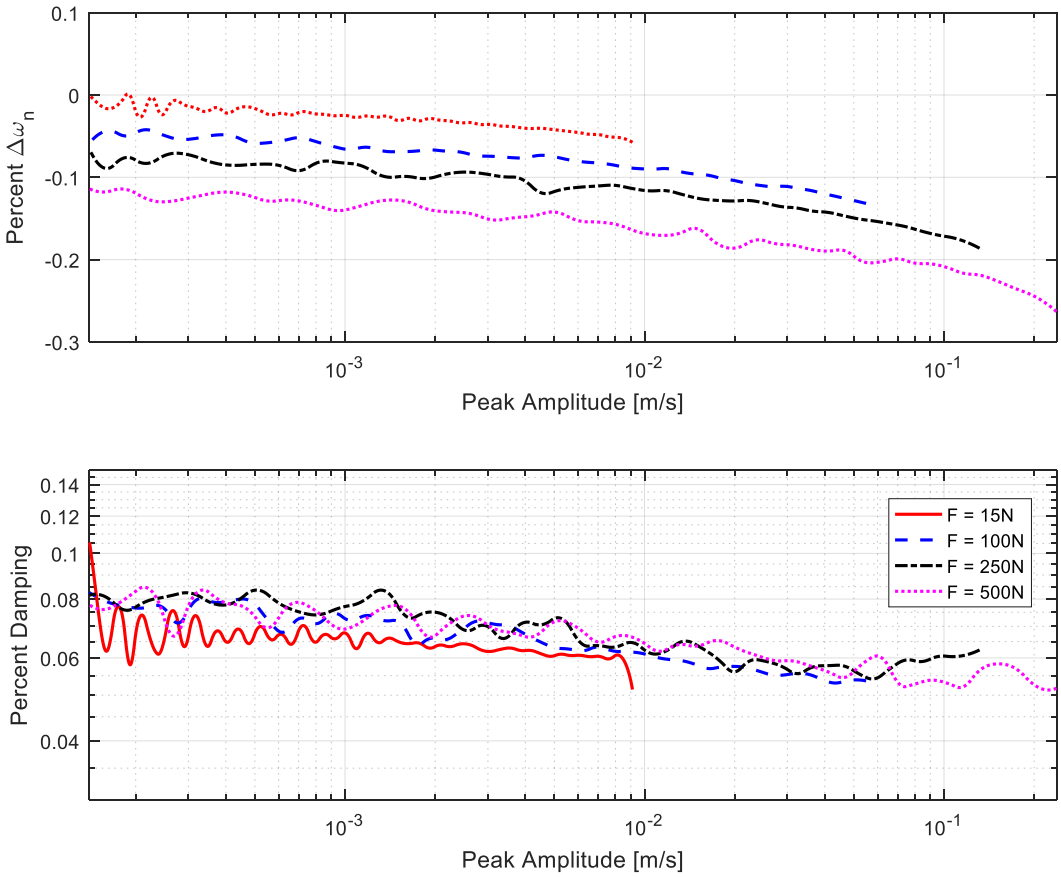

Figure A.1: *Mode 1 at 10.2 Nm torque for B1-B2*

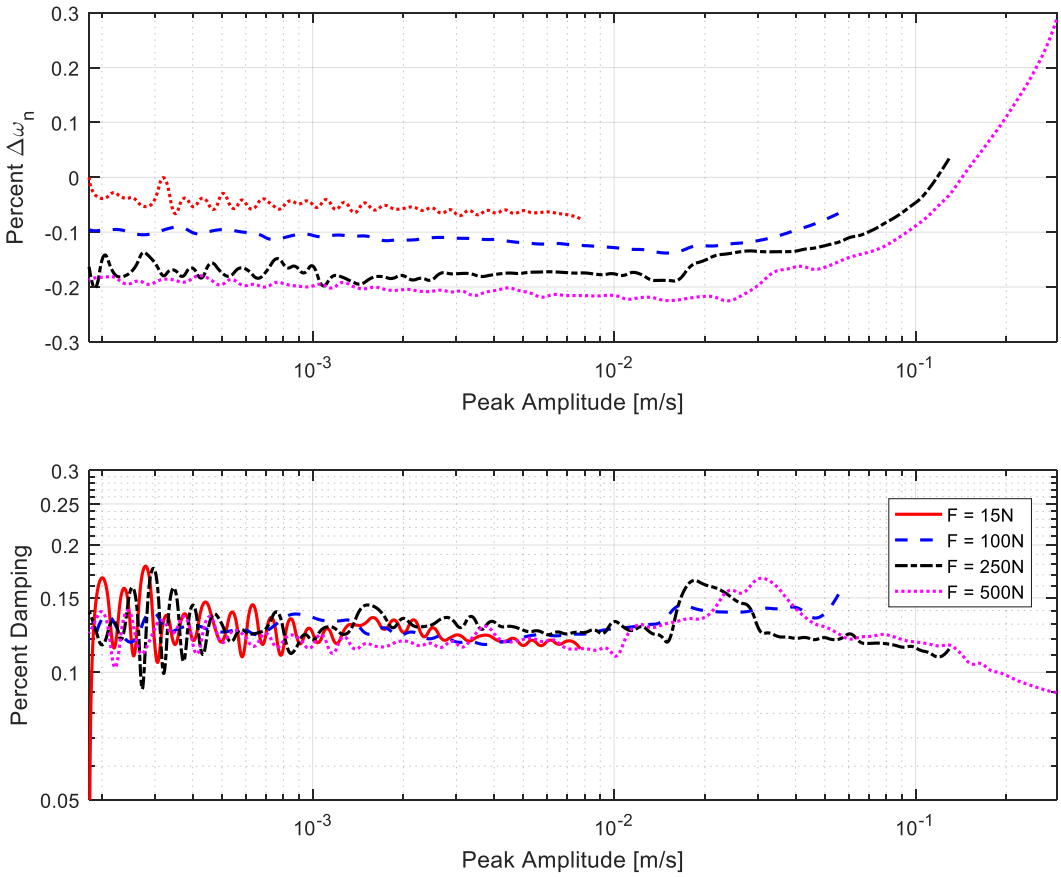

Figure A.2: *Mode 1 at 10.2 Nm torque for B5-B6*